

Effect of Wind Speed on the Performance of Troposkein Vertical Axis Wind Turbine

Unnikrishnan Divakaran*, V. Ratna Kishore*[‡], Ajith Ramesh*

*Department of Mechanical Engineering, Amrita School of Engineering, Coimbatore, Amrita Vishwa Vidyapeetham, India.

(d_unnikrishnan@cb.amrita.edu, v_ratnakishore@cb.amrita.edu, r_ajith@cb.amrita.edu)

[‡]Department of mechanical Engineering, Amrita School of Engineering, Coimbatore, Amrita Vishwa Vidyapeetham, Tamilnadu, India, Pin code: 641-112 Tel: +91 422 268 5000, v_rathnakishore@cb.amrita.edu

Received: 29.06.2019 Accepted: 14.08.2019

Abstract- Wind energy being one of the renewable energy sources, having potential to substitute power generation from fossil fuels, has always drawn the spot light of research society. Non-straight bladed vertical axis wind turbine (VAWT) has proven to be one among the better options among small scale turbines. The presented work investigates the effect of wind speed on the performance of a Troposkein blade VAWT using 3D CFD simulations. The transitional SST K- ω model is used for modeling turbulence. Simulations are conducted for varying wind velocities (6 m/s - 14 m/s) and varying tip speed ratios (TSR) (1.8 - 2.7). Based on the swept area of the turbine, the mean radius of the turbine is calculated which serves as the basis for the calculation of TSR. The results obtained indicate that the turbine performance is significantly affected at lower TSR at varying wind speeds, and the percentage of change is much lower at higher TSR values. Peak performance of the turbine is noted at the same TSR value for all wind velocities, and the magnitude of coefficient of performance is found to be almost the same.

Keywords VAWT, Troposkein blade, wind speed.

1. Introduction

To cater to the ever-increasing demand for energy, technology has always come up with unique solutions. Still, humanity's thirst for more is never catered. The energy available in different forms is generally harnessed and converted to either mechanical or electrical forms. The increased dependency on fossil fuels has led to catastrophic environmental problems like pollution. Therefore, the increase in demand for energy has forced the scientific community to search for other alternate sources of energy. One such major reliable source has been wind, which when converted to mechanical or electrical forms have always been a popular source of renewable energy.

Based on the orientation of the rotation axis with respect to wind direction, wind turbines can be categorized into two, i.e. Horizontal axis wind turbines (HAWT) and Vertical axis wind turbines (VAWT). At present, most of the commercial wind turbines are HAWTs due to their higher efficiency when compared to the VAWTs [1-3]. Improvement in performance and efficiency can be attributed to higher investments in the development of wind turbine technology which has been focused on HAWT for the past two decades [1]. Hence, the advantages of VAWT, like; lower operational

wind speed, high tolerance to the turbulence level of the wind, omni-directionality, placement of generator on the ground [4-8], etc., have been overlooked. These advantages, off late, have expanded the field of applicability of VAWTs, and hence, the same is reflected in their recent popularity.

The classification of VAWT is based on the forces which causes the wind turbine to rotate, namely the lift type (Darreius) and the drag type (Savonius) [9]. Further, the lift force based VAWT can be classified based on the shape of the blades, like straight (H-Type) and non-straight Troposkein, Canted, and Helical, to name a few. The work on H-type Darreius turbines have been mostly focused on the geometrical aspects like number of blades [10-12], airfoil shape [13-15], solidity (σ) [16-18], blade pitch angle [19] and turbine shaft [20] and operational parameters like tip speed ratio (TSR) (λ) [21-26], turbulence intensity [24, 27-29] and Reynolds number [22, 30-33].

A detailed experimental analysis was performed on a three bladed high solidity ($\sigma = 0.45$) VAWT by McLaren [34], to study the effect of wind velocity, pre-set pitch angle, chord length and airfoil, on the performance of a wind turbine. They have accurately measured aerodynamic loading using strain gauge-based force measurement on the

strut and torque measurement from the shaft. The wind velocity was varied from 6 to 11 m/s. Coefficient of performance was almost similar from 8 to 11 m/s and consistently lower by about 12%. Elkhoury et al.[35] has performed experiments on a three bladed H-Type VAWT with chord 200 mm, turbine diameter 800 mm ($\sigma = 0.75$) and for NACA0018 and NACA 634-221 airfoil profiles. The experiments were conducted for a wind velocity range of 4 m/s to 10 m/s. The peak coefficient of performance for the entire studied wind velocity range is occurring at the same tip speed ratio, and variation in CP was found to be less than 3% for various tip speed ratios. Li et al.[36] investigated the performance of straight bladed VAWT both in wind tunnel and infield. The wind turbine is two bladed with chord 0.265 m and rotor diameter 2 m ($\sigma = 0.265$) with NACA0021 airfoil. They examined the effect of blade pitch angle, wind velocity and Reynolds number, on the performance of VAWT. The Reynolds number study in wind tunnel shows that as chord Reynolds number increases, the coefficient of power increases, and the peak coefficient of power occurs at the same tip speed ratio. The field experiments with fluctuating wind condition revealed that the performance of the wind turbine is significantly varying for tip speed ratios greater than 2. For almost every experiment conducted in the above mentioned studies, influence of TSR and wind velocity on the performance was studied.

Rezaeiha et al. [8, 19, 20, 37] have used 4-equation transitional SST k- ω model for a two-bladed VAWT to study the effect of pitch angle, presence of shaft, the effect of solidity (constant Reynolds number) and effect of various other operational parameters (constant Reynolds number). Lohry and Martinelli [38] have performed 2D and 3D computations of performance of VAWT with varying blade aspect ratio (3 to 20) and solidity (0.13 to 0.79). It is concluded that the performance of the turbine improves for larger radius while maintaining the same solidity. Need for 3D simulations is well emphasized by Bhargav et al. [39] in their numerical work to study the effects of fluctuating wind conditions. Their study involves a three-bladed high solidity VAWT of 450 mm chord, 3 m height and 2.7 m in diameter. In a 2D numerical work by Chandramouli et al. [40] the effect of pitch angle on the performance was studied in variable wind velocities and variable TSR. It was found that negative pitch performed better in all the conditions studied.

The popularity of H-Type Darrieus VAWT is because of simplicity in terms of manufacturing. However, the torque ripples and bending moment stress on the structure is found to be higher for the H-Type Darrieus VAWT [8]. These disadvantages of the straight blade have driven research in exploring better designs. Troposkein blade, being one among the designs which have zero bending moment, will have less structural issues. A study on canted blades by Armstrong et al. [23] shows similar performance concerning straight blade VAWTs at same TSR. In an optimisation work done by Bedon et al. [41], they obtained optimal chord to attain better power coefficient and better power output. The wind velocity for his study was 9 m/s and 12 m/s respectively for improved power coefficient and power output respectively. The shape of the blade in the work was described as Straight-Circular-Straight. Methods like variable chord length along the blade

for troposkien turbines has been examined numerically to improve the performance of the turbine [42]. Delafin et al. employed streamtube models, vortex methods and CFD with existing experiments for a 3D full-scale VAWT to determine its performance. The study compares different computational models for the full-scale turbine used in experiments performed at Sandia National Laboratories in the 1980s [43].

The effect of wind velocity on the performance of a straight blade VAWT has been studied with respect to two different aspects; for a constant chord Reynolds number and for a constant wind velocity. The performance of the wind turbine (C_p) has shown a significant dependence on TSR and less dependent of wind speed. Most of the work available in the literature were on straight bladed VAWT but studies on non-straight bladed VAWTs, in order to understand the effect of various geometric and operating conditions on performance are limited [15-17]. Also, it is interesting to study the effect of wind speed on non-straight bladed VAWT like Troposkien VAWT as relative velocity of the turbine blade would vary along its length.

The present work focuses on the numerical analysis of a 3D troposkien bladed VAWT model under different wind conditions (6m/s to 14m/s). The TSR (λ) based on the mean radius was varied from 1.8 to 2.7. The turbine performance was evaluated based on coefficient of performance. Also, in order to understand the nature of wind turbine performance detailed flow analysis was done.

2. Computational Model

The flow velocities that are studied are much below the velocity of sound, hence the working fluid, the air is assumed to be incompressible. For a three-dimensional incompressible isothermal flow, the conservation of mass (continuity) and momentum (Navier-Stokes) equations are solved along with the turbulence model. Transition, SST k- ω model, was used to model the turbulence because the Reynolds number of flow over the airfoils for various wind velocities and tip speed ratios were found to be in the range of 1.4×10^5 to 3.5×10^5 . Moreover, the four equation Transition SST k-w model has been used by several researchers [8, 40, 44-50] for modelling VAWT and results were found to be validating well with the experimental data. The governing equations for the present model are given in equations 1 - 6.

$$\nabla \cdot \vec{V} = 0 \quad (1)$$

$$\rho \frac{D\vec{V}}{Dt} = -\nabla p + \mu \nabla^2 \vec{V} \quad (2)$$

$$\rho \left[\frac{\partial(k)}{\partial t} + \frac{\partial(U_j k)}{\partial x_j} \right] = \hat{P}_k - \hat{D}_k + \frac{\partial}{\partial x_j} \left[(\mu + \sigma_k \mu_t) \frac{\partial k}{\partial x_j} \right] \quad (3)$$

$$\rho \left[\frac{\partial(\omega)}{\partial t} + \frac{\partial(U_j \omega)}{\partial x_j} \right] = P_\omega - D_\omega + \frac{\partial}{\partial x_j} \left[(\mu + \sigma_\omega \mu_t) \frac{\partial \omega}{\partial x_j} \right] + 2(1 - F_1) \frac{\rho \sigma_{\omega 2}}{\omega} \frac{\partial k}{\partial x_j} \frac{\partial \omega}{\partial x_j} \quad (4)$$

$$\rho \left[\frac{\partial(\gamma)}{\partial t} + \frac{\partial(U_j \gamma)}{\partial x_j} \right] = P_\gamma - D_\gamma + \frac{\partial}{\partial x_j} \left[\left(\mu + \frac{\mu_t}{\sigma_f} \right) \frac{\partial \gamma}{\partial x_j} \right] \quad (5)$$

$$\rho \left[\frac{\partial(\hat{R}e_\alpha)}{\partial t} + \frac{\partial(U_j \hat{R}e_\alpha)}{\partial x_j} \right] = P_\alpha + \frac{\partial}{\partial x_j} \left[(\sigma_\alpha (\mu + \mu_t)) \frac{\partial \hat{R}e_\alpha}{\partial x_j} \right] \quad (6)$$

Where ρ is the density, V is the velocity, μ is the dynamic viscosity, p is the pressure, \hat{P}_k , P_ω , P_γ , P_α is the production terms for respective quantities, \hat{D}_k , D_ω , D_γ are destruction terms of the respective quantities.

The geometrical features of the computational domain are represented in table 1. The domain is modelled using two sub domains; one to capture the rotational motion near the turbine and an external domain which is stationary, as shown in Fig. 1(a). The dynamic motion of the turbine blade during the turbine operation is captured with the rotating domain. A symmetric model was developed for reducing computational time and effort.

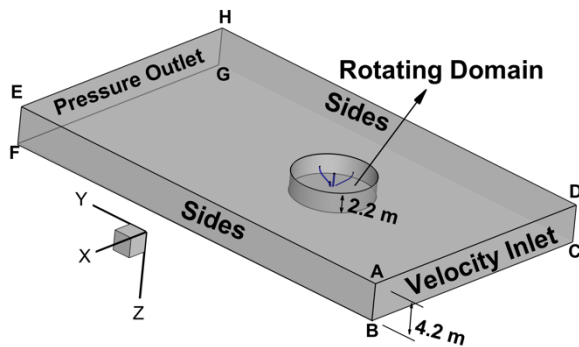


Fig. 1 (a) Domain geometry and boundary conditions

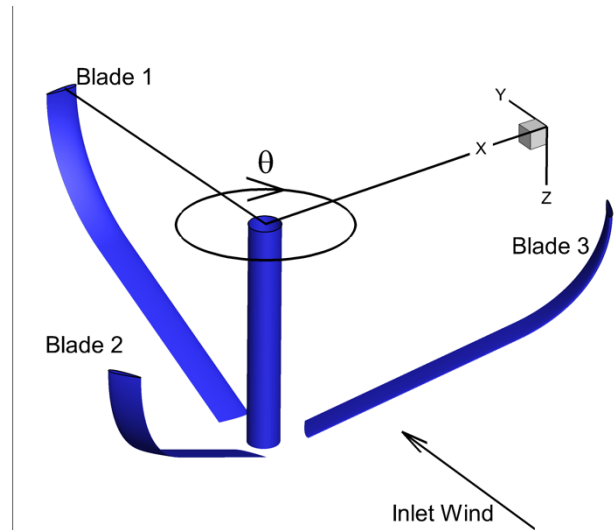


Fig. 1 (b) Wind turbine model studied in the present work

GAMBIT 2.4 is used for modelling and meshing of the domain, a 3D representation of which is displayed in Fig. 1(a). A NACA0015 airfoil profile of chord length 210 mm with the trailing edge rounded was generated. The Troposkien blade geometry was generated by sweeping the airfoil cross section along the straight – circular – straight line as shown in Fig. 1(b). Each blade cross section has 340 grid points to ensure that the flow separations, if any, is appropriately captured. Fine surface meshes (shown in Fig. 2(a)) are generated on all the airfoils and shaft in order to capture the aerodynamic effects adequately. Grid density of the surface mesh near the tip is kept higher in order to accurately model the tip effects (shown in inset of Fig. 2(a)). In order to capture the flow features closer to the surface of the blade and shaft, boundary layer mesh is defined with the first length of 2.5×10^{-5} m, and a growth ratio of 1.35 with 21 layers. To capture the rotational effects of the turbine, a cylinder of radius 2.5 m is created, encompassing all the blades and shaft. Vertical symmetry is ensured throughout the modelling so as to reduce the computational effort. An outer stationary domain (shown in Fig. 2(b)) similar to McLaren's [1] is generated, which has a cylindrical hole to fit the inner rotating domain. Approximately 11.5 million cells are generated in the entire process of meshing.

Table 1 Geometrical details and operating conditions of the turbine in the present work

Blade profile	NACA 0015
Chord, c	0.210 m
Mean Diameter of the rotor, D (based on swept area)	2.7 m
The frontal area of the rotor	8.1 m ²
Solidity based on mean diameter, σ	0.5
Number of blades, N	3
Wind speed, U_∞	6 – 14 m/s

As shown in Fig. 1(a), the solid walls like blades and shaft were set to 'no slip'. The entry was set as velocity inlet through the surface ABCD at 10 m/s wind velocity, and the

exit was set as pressure outlet at 1 atm pressure at surface EFGH as shown in Fig. 1(a). The initial condition and the inlet condition was set the same at 10m/s. All the simulations were run at a free stream velocity of 10 m/s and at 5% turbulence intensity. Based on the swept area of the turbine, the mean radius of the turbine was calculated which serves as the basis for calculation of TSR. TSR is varied from 1.6 to 2.9 to effectively study the performance parameters.

The simulations were done in ANSYS FLUENT 15.0. The time step used for the computation is equivalent to 1° of turbine rotation. Each simulation was performed for 10 to 12 rotations. It was observed that for most of the computations flow around the wind turbine becomes periodic at the end of the 9th rotation. Mean C_m and C_p data was found to be varying less than 0.2% for 9th and 10th rotation. Hence results of the 12th rotation have been analyzed in the present work.

The grid domain and solution methodology has been followed based on our previous numerical studies [40]. Using ANSYS FLUENT, this solution methodology has been validated from straight bladed Darrius wind turbine of McLaren et.al. [32] experimental study

3. Grid and Time step independence

The numerical solution should be independent of simulation parameters such as mesh size and time step duration. Simulations have been carried out to prove the same classic conditions of $U_\infty = 10 \text{ m/s}$ and $TSR (\lambda) = 2$. Fig. 3 shows the time step independence of the solution for $\lambda = 2$ and velocity 10 m/s. Time steps were calculated based on the degrees of rotation of the turbine. The numerical analysis with a time resolution equivalent to 2 degree, 1 degree and 0.5 degree were performed. It can be seen that moment coefficient for blade 1 with 1 degree time step matches well with 0.5 degree time step indicating the solution is time step independent. Hence, in the present work all the computations are performed with 1 degree time step.

Grid independence study was conducted in order to decide on the maximum number of grid points that can be used for the study. It was found that the grid of 11.5 million could predict the results at fairly reasonable accuracy. Table 2 represents the grid independence study for a sample case of TSR 2 with wind velocity of 10 m/s.

Table 2 Grid independence study

Sl. No.	No. of Grid points	C_p predicted
1	9×10^6	0.2034
2	11.5×10^6	0.2091
3	17×10^6	0.2094

4. Results and Discussion

In the presented work, simulations are performed on a three bladed troposkien vertical axis wind turbine for different wind speeds and TSR. The wind velocity range (6 – 14 m/s) was selected based on the real time wind available in any

urban environment [2]. The performance of vertical axis wind turbine was found to be at its best in the range of TSR varying from 1.8 to 2.7[3].

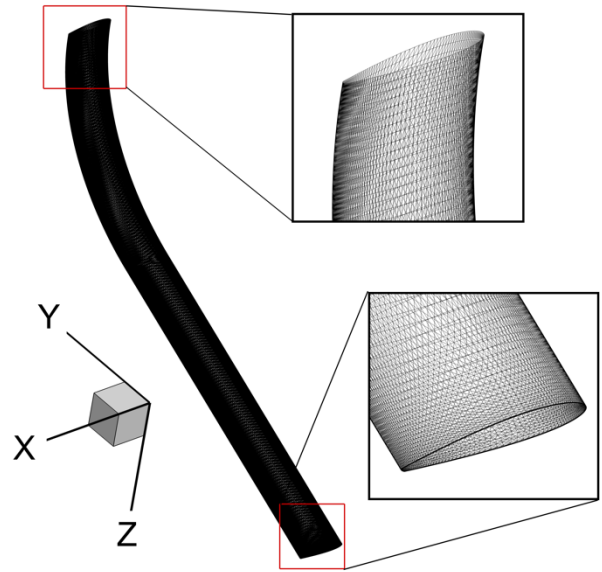


Fig.2(a) surface mesh on the blade

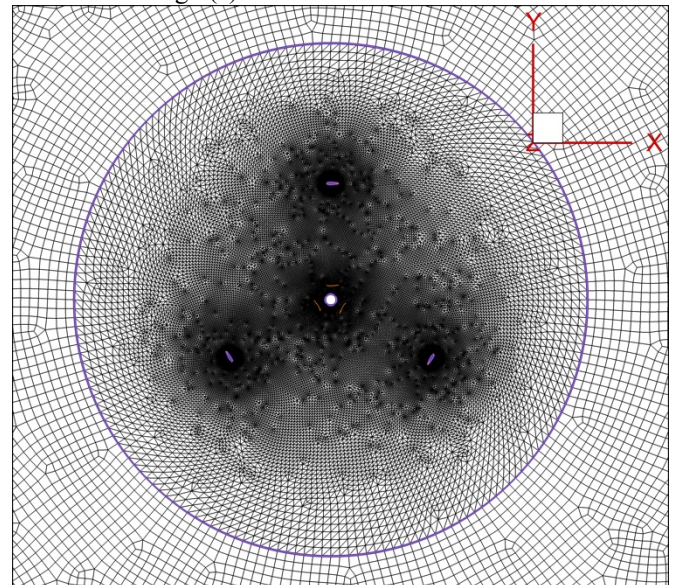


Fig. 2(b) Mesh on the symmetric plane

Fig. 4(a) represents the variation of c_m for each blade versus no of cycles. The first three cycles have significant effects due to the initial condition. It was noticed that after eight cycles the value of C_m has achieved cyclic nature. Therefore, for every simulation that was performed, the value of C_m was obtained only after 12 complete cycles of rotation by the turbine.

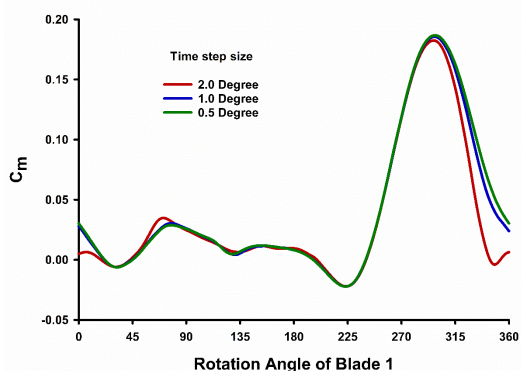


Fig. 3. Blade 1 C_m variation as a function of rotation angle for various time steps at velocity 10 m/s and TSR 2

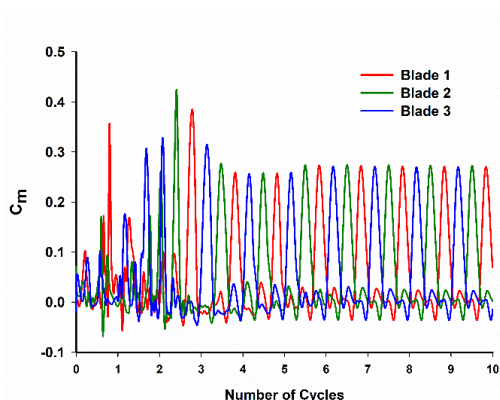


Fig. 4(a) Cyclic Nature of C_m over 10 cycles of a Troposkien bladed VAWT running at $\lambda = 2.3$ and $v = 10$ m/s

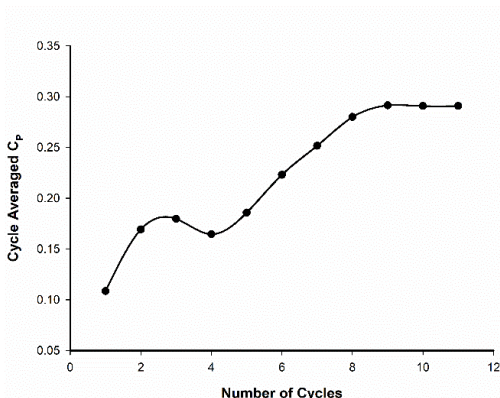


Fig. 4(b) Averaged C_p value for 10 cycles for troposkien bladed VAWT running at $\lambda = 2.3$ and $V = 10$ m/s

The cycle averaged C_p data plotted against no of cycles shown in Fig. 4(b). The C_m plot appears to have achieved statistical cyclic nature after five cycles, but the average C_p value keeps varying. Hence it is essential to run the simulations for more than nine cycles. All the simulations

run for the presented study are run for a minimum of 12 cycles in order to avoid any transitional effects.

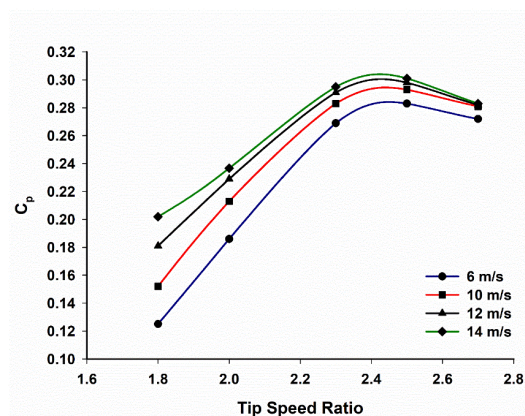


Fig. 5 Variation of C_p with respect to TSR and wind velocity

From Fig. 5, it can be observed that for various wind velocities, the range of tip speed ratios at which peak occurs, remains the same. The overall trend of the performance remains the same irrespective of the wind velocities. For lower wind velocities, it can be noted that there is a 66% improvement in the performance when wind velocity is increased by 1.3 times. This may be attributed to the lesser interaction of the wake leaving the preceding blade surface on the incoming blade. It is also to be noted that when TSR was increased beyond a threshold value of 2.5, the difference in the performance coefficient is very less. These observations further strengthen the impression of having lesser wake interaction on the incoming blade.

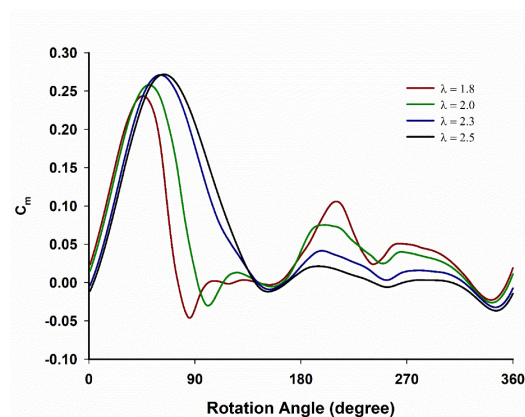


Fig. 6 Effect of TSR on C_m in one complete rotation of a blade.

It may be noted from Fig. 6 that the maximum C_m occurs in between 0° and 90° and the secondary effects are visible at 180° and 270° of the rotation angle of blade 1. It is observed that irrespective of the TSR, the energy that can be extracted from the wind remains in the same range of rotation angles. It is also observed that an increase in TSR shifts the peak slightly towards higher angle. This may be due to lesser interaction of wakes from the preceding blade hitting the incoming blade.

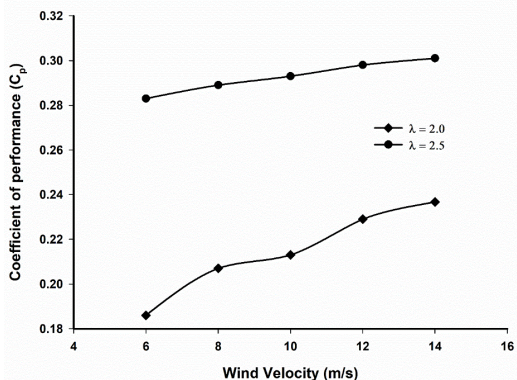


Fig. 7 Effect of wind velocity on the performance of troposkein blade VAWT against two different TSR

If we compare the performance of the wind turbine across TSR values, for variable velocity, it is understood that for lower TSR the performance is poor when compared to higher TSR. From Fig. 7 it can be inferred that for higher TSR and higher velocity, the difference in performance coefficient becomes lesser. It was observed that the difference in the performance of the same turbine under different TSR for same wind velocity is higher at lower wind velocity and lower in higher wind velocity. This may be accounted to the reduced interaction of the vortex shed by one blade over the next incoming blade.

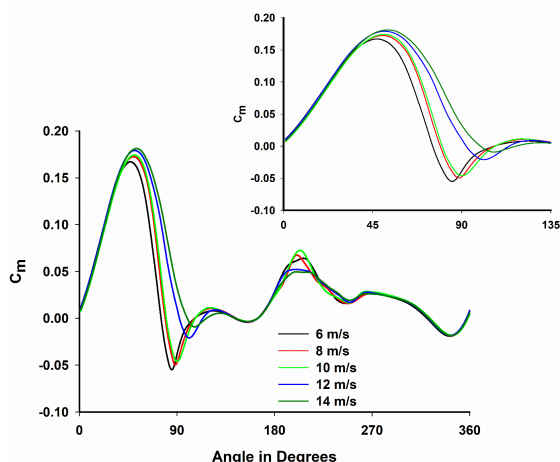


Fig. 8 Variation of Coefficient of moment with respect to rotation angle for various wind velocities at TSR = 2

The C_m data taken for the lower TSR values ($\lambda = 2$), depicted in Fig. 8, shows that as velocity increases the peak broadens and the effects of secondary interaction becomes prominent. The peak pattern is found to occur in the same range of rotation angle for all velocities.

On the contrary, if we take the C_m data of higher TSR ($\lambda = 2.5$), from the Fig. 9, it is evident that the peak occurs at the same rotation angle and follows the same trend across the velocity range considered. This may be attributed to lesser interaction of the blade vortex on the oncoming blade. The secondary effects are also negligible in higher TSR.

It is interesting to note that the moment coefficient does not differ much for a single blade even though the velocity of incoming wind is changed. It gives sufficient confidence on the numerical model used for the prediction of performance.

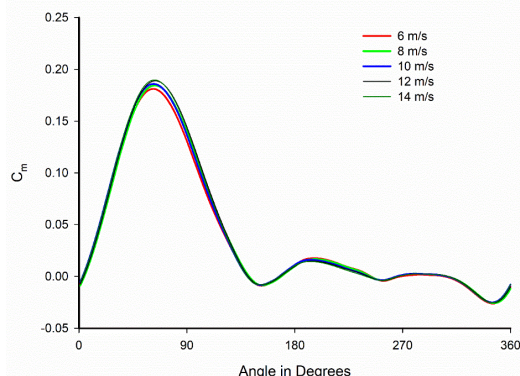


Fig. 9 Variation of Coefficient of moment with respect to rotation angle for various wind velocities at TSR = 2.5

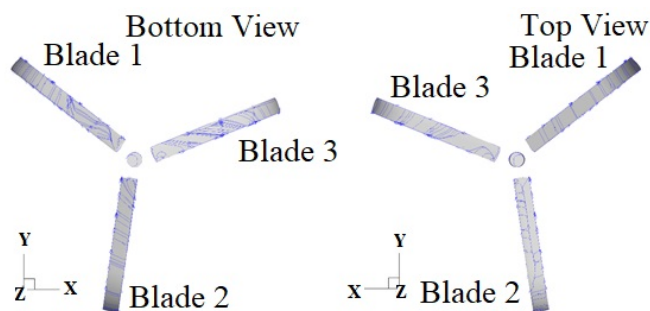


Fig. 10 skin friction lines over the blades for TSR $\lambda = 2$, velocity 14 m/s

The flow over the blades of the troposkien blade wind turbine is depicted using skin friction lines as shown in Fig. 10. The wind velocity for the simulation was set to be in the positive y direction. The flow over the blade in top view and bottom view are shown in Fig. 10 for a wind velocity of 14 m/s and TSR = 2. Also, the Fig. shown was for the azimuth angle when maximum moment coefficient occurs for the blade 2. From the Fig, it is clearly seen that on the pressure side of blade 2 the flow is almost stream lined and at the suction side the flow separates from the blade surface.

In order to corroborate the findings from skin friction lines pressure and vorticity magnitude contours were plotted. Fig. 11 showcases (a) the pressure profiles, (b) vorticity magnitudes, at three sections of the turbine; Symmetric section ($h = 0$ m), Mid-section ($h = 0.75$ m) and tip section ($h = 1.325$ m). The views are zoomed to ensure the pressure profiles / vorticity contours are legible in their corresponding sections. The coordinates represent the x and y coordinates of the section plane. It must be noted that the symmetry plane lies at $z = 0$. The pressure on blade 2 and blade 1 has sharp contrast in their values in the pressure side and suction side. This significantly contributes in generating lift force on those

blades. It is noted here that the pressure drop near the tip is very negligible. In the vorticity contours at the mid section, it can be seen that the vorticity interaction between blades are not as significant as symmetric and tip sections. Whereas when it comes near to the tip the wake interaction between the tip vortices are really high. This supports the non alignment of skin friction lines near the tip. The wakes generated by the shaft also influences the flow over the blades, but only near the tip of the turbine blade.

Fig. 12 (a), (b) and (c) represents the pressure plots for wind velocity 8 m/s, 10 m/s and 14 m/s respectively. All the static pressure contours are plotted on the same scale (i.e., -50 to 50 Pa) in order to compare the results. With the increase in wind velocity, the pressure difference between suction side and pressure side increases leading to higher lift force and hence better power production. On observation of these contours it is clear that the trend of pressure drops are similar in the same height section.

Fig. 13 (a), (b) and (c) represents the vorticity magnitude contours for wind velocity 8 m/s, 10 m/s and 14 m/s respectively. The contours also follow similar trend as that of the pressure profiles. As the wind velocity increases the vorticity effects become significant. The wake interaction at the tip of the turbine blade is very significant at higher wind velocities.

5. Conclusions

The effect of wind speed on the performance of a troposkien wind turbine was studied numerically using the commercial code – FLUENT. All simulations were conducted in 3D with SST $k-\omega$ turbulence model for different wind velocities (6 m/s – 14 m/s) and different TSR values (1.8 to 2.8). The following are the conclusions drawn:

- To parametrize the study, TSR values were calculated based on the mean radius of the turbine. In reality, the blade diameter is different at different sections of height. Due to this reason, there is a significant change in the pressure profiles and it is evident from the pressure contours as well.
- The turbine performance is significantly affected at lower TSR at different wind speeds. The percentage of change in coefficient of performance is much lower at higher TSR values when compared to lower TSR. The peak performance is almost similar at higher TSR. It is corroborated by the C_m curves at higher TSR, which got superimposed on each other, leaving minimal difference.
- Near to the symmetric plane of the turbine, the pressure difference between suction and pressure side is significant, and for a section away from the symmetry, the pressure difference is found to be reducing.

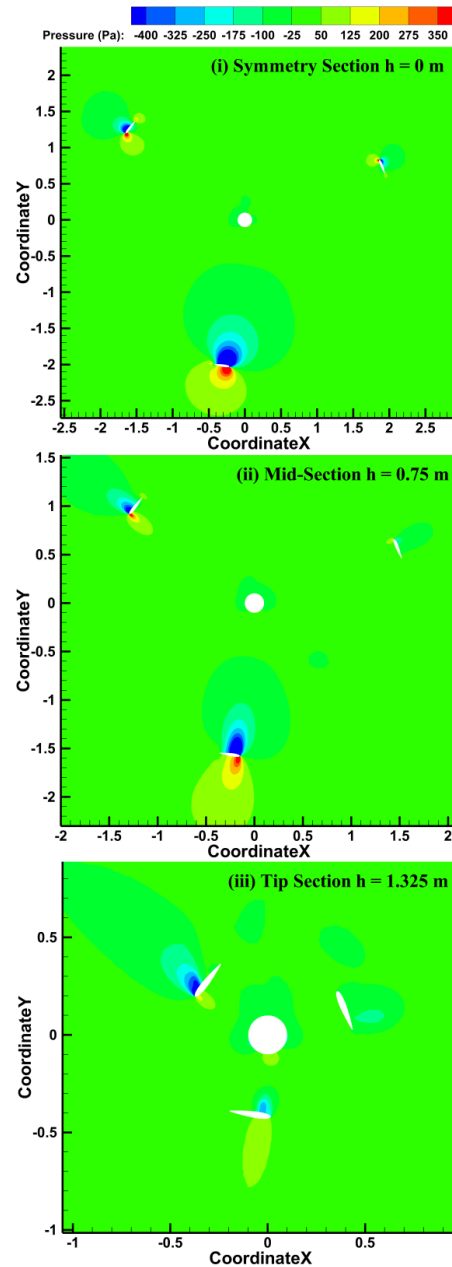


Fig. 11 (a) Pressure profiles at symmetric section, Mid-section and Tip section

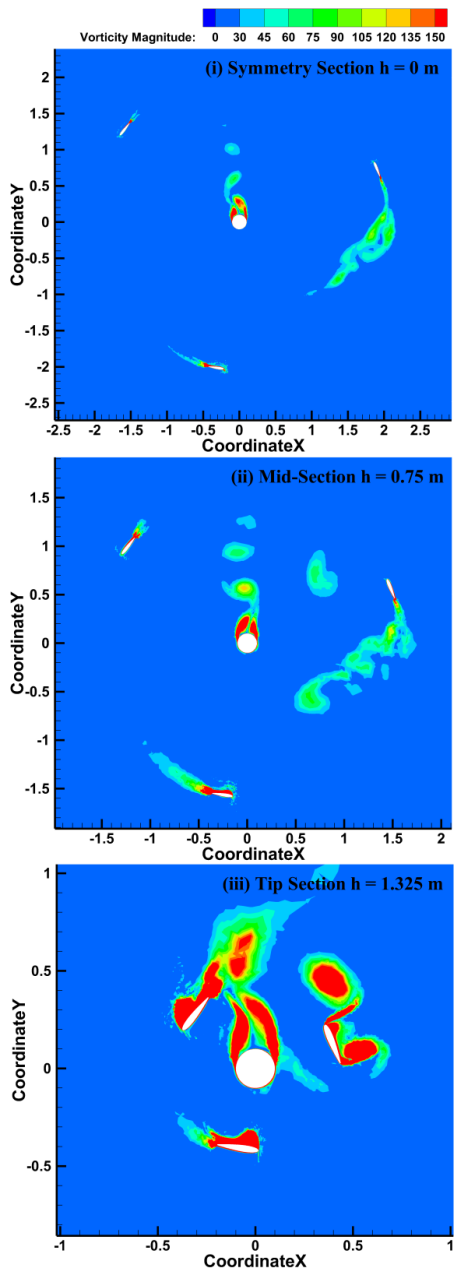


Fig. 11 (b) Vorticity magnitude at symmetric section, Mid-section and Tip section

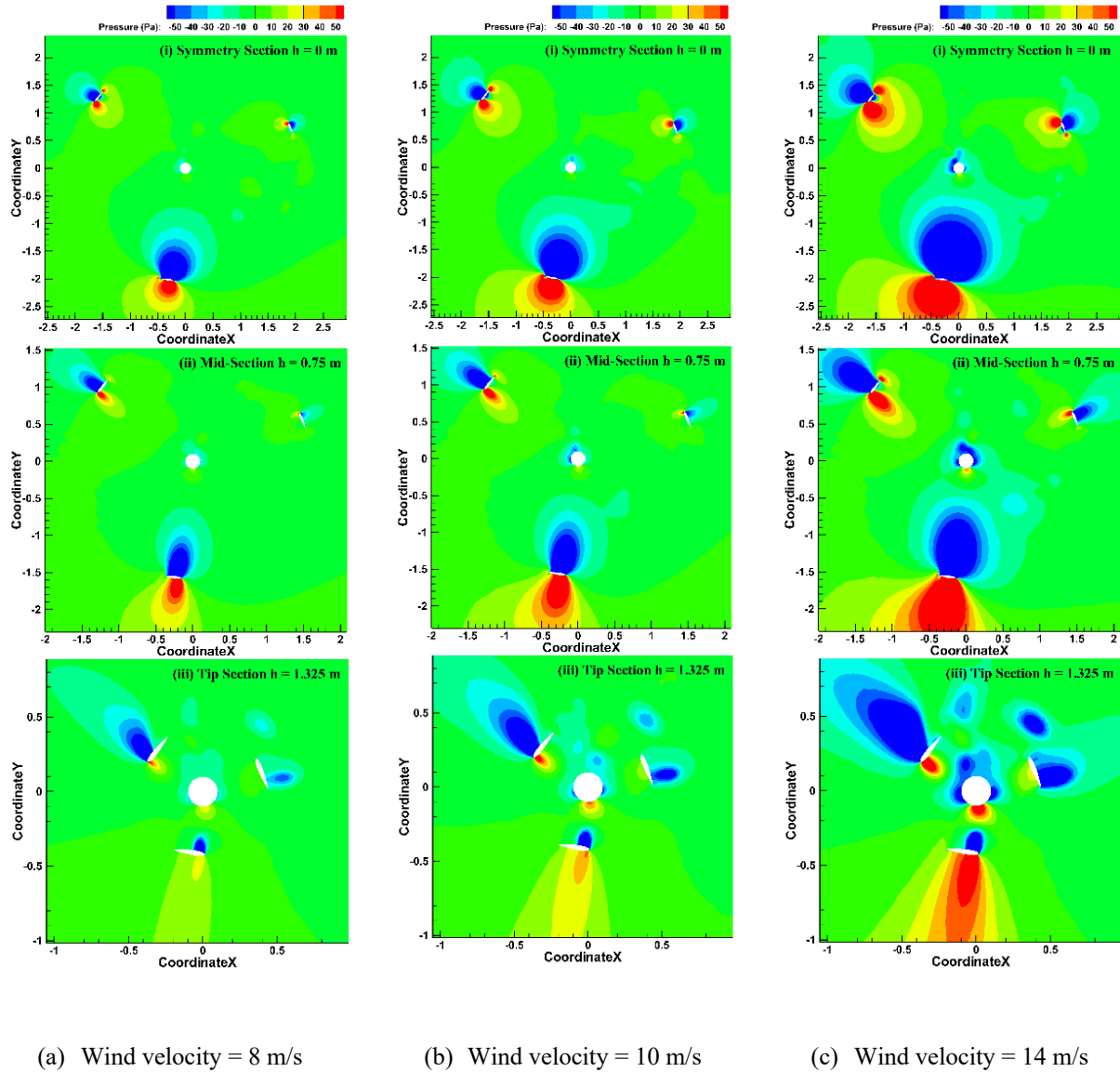


Fig. 12 Pressure contours at TSR = 2 at symmetric ($h = 0$ m), mid ($h = 0.75$ m) and tip ($h = 1.325$ m) section heights

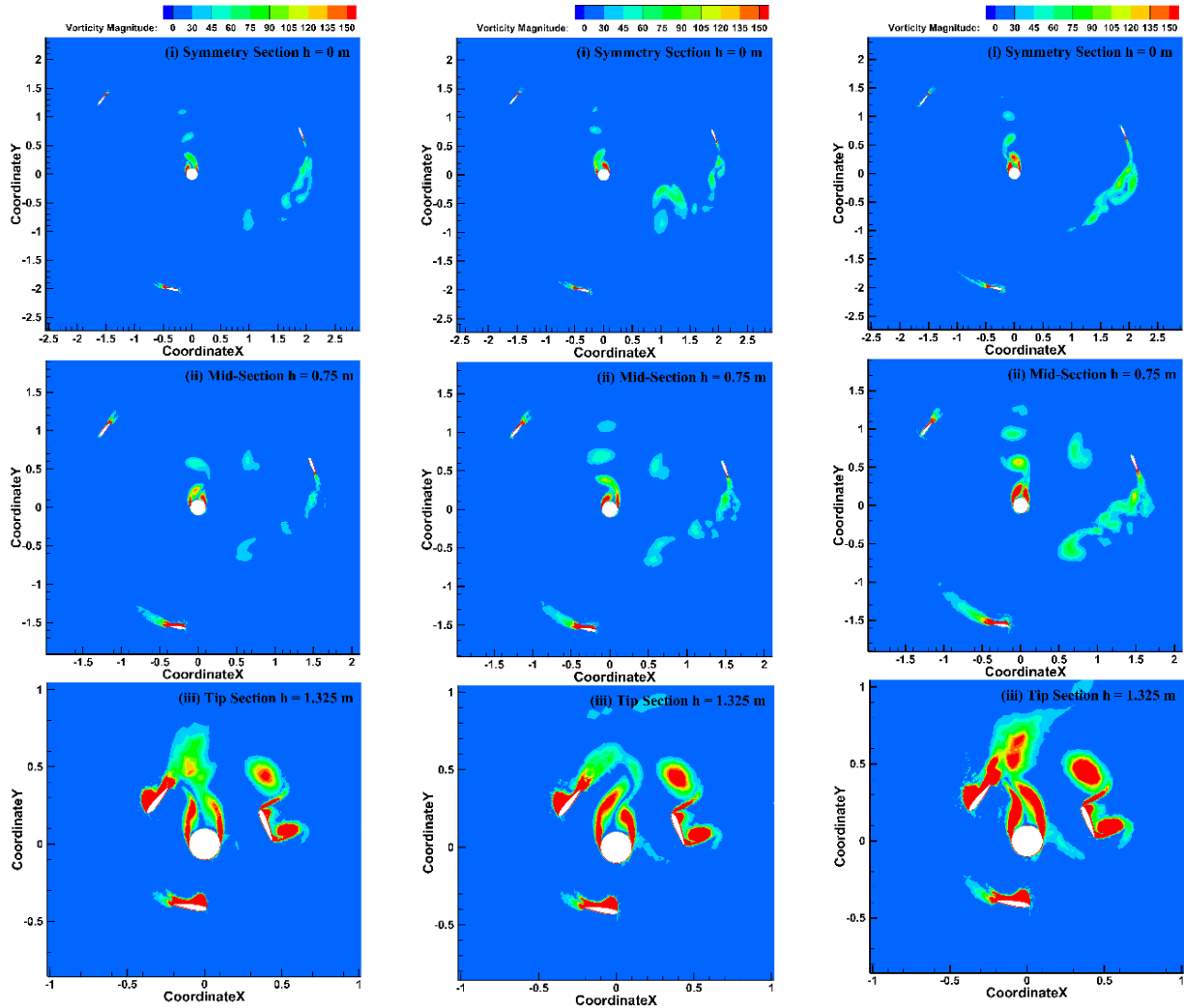


Fig. 13(a) Vorticity contour for velocity 8 m/s and $\lambda = 2$

Fig. 13(b) Vorticity contour for velocity 10 m/s and $\lambda = 2$

Fig. 13(c) Vorticity contour for velocity 14 m/s and $\lambda = 2$

References

- [1] Eriksson, S., H. Bernhoff, and M. Leijon, *Evaluation of different turbine concepts for wind power*. Renewable and Sustainable Energy Reviews, 2008. **12**(5): p. 1419-1434.
- [2] Wendler, J., D. Marten, G. Pechlivanoglou, C.N. Nayeri, and C.O. Paschereit. *An unsteady aerodynamics model for lifting line free vortex wake simulations of hawt and vawt in qblade*. American Society of Mechanical Engineers.
- [3] Borg, M. and M. Collu, *A comparison between the dynamics of horizontal and vertical axis offshore floating wind turbines*. Phil. Trans. R. Soc. A, 2015. **373**(2035): p. 20140076.
- [4] Owens, B.C. and D.T. Griffith. *Aeroelastic stability investigations for large-scale vertical axis wind turbines*. IOP Publishing.
- [5] Paulsen, U.S., H.A. Madsen, J.H. Hattel, I. Baran, and P.H. Nielsen, *Design optimization of a 5 MW floating offshore vertical-axis wind turbine*. Energy Procedia, 2013. **35**: p. 22-32.
- [6] Mertens, S., *Wind energy in urban areas: Concentrator effects for wind turbines close to buildings*. Refocus, 2002. **3**(2): p. 22-24.
- [7] Shires, A., *Design optimisation of an offshore vertical axis wind turbine*. Proceedings of the ICE-Energy, 2013. **166**(EN1): p. 7-18.
- [8] Rezaeiha, A., H. Montazeri, and B. Blocken, *Characterization of aerodynamic performance of vertical axis wind turbines: impact of operational*

- parameters. *Energy Conversion and Management*, 2018. **169**: p. 45-77.
- [9] Savonius, S.J., *Wind rotor*. 1930, Google Patents.
- [10] Cheng, Z., H.A. Madsen, Z. Gao, and T. Moan, *Effect of the number of blades on the dynamics of floating straight-bladed vertical axis wind turbines*. *Renewable Energy*, 2017. **101**: p. 1285-1298.
- [11] Delafin, P.L., T. Nishino, L. Wang, and A. Kolios, *Effect of the number of blades and solidity on the performance of a vertical axis wind turbine*. *Journal of Physics: Conference Series*, 2016. **753**: p. 022033.
- [12] Li, Q.a., T. Maeda, Y. Kamada, J. Murata, K. Furukawa, and M. Yamamoto, *Effect of number of blades on aerodynamic forces on a straight-bladed Vertical Axis Wind Turbine*. *Energy*, 2015. **90**: p. 784-795.
- [13] Bedon, G., S. De Betta, and E. Benini, *Performance-optimized airfoil for Darrieus wind turbines*. *Renewable Energy*, 2016. **94**: p. 328-340.
- [14] Ferreira, C.S. and B. Geurts, *Aerofoil optimization for vertical-axis wind turbines*. *Wind Energy*, 2014. **18**(8): p. 1371-1385.
- [15] Sengupta, A.R., A. Biswas, and R. Gupta, *Studies of some high solidity symmetrical and unsymmetrical blade H-Darrieus rotors with respect to starting characteristics, dynamic performances and flow physics in low wind streams*. *Renewable Energy*, 2016. **93**: p. 536-547.
- [16] Eboibi, O., L.A.M. Danao, and R.J. Howell, *Experimental investigation of the influence of solidity on the performance and flow field aerodynamics of vertical axis wind turbines at low Reynolds numbers*. *Renewable Energy*, 2016. **92**: p. 474-483.
- [17] Li, Q.A., T. Maeda, Y. Kamada, J. Murata, K. Shimizu, T. Ogasawara, A. Nakai, and T. Kasuya, *Effect of solidity on aerodynamic forces around straight-bladed vertical axis wind turbine by wind tunnel experiments (depending on number of blades)*. *Renewable Energy*, 2016. **96**: p. 928-939.
- [18] Li, Q.A., T. Maeda, Y. Kamada, K. Shimizu, T. Ogasawara, A. Nakai, and T. Kasuya, *Effect of rotor aspect ratio and solidity on a straight-bladed vertical axis wind turbine in three-dimensional analysis by the panel method*. *Energy*, 2017. **121**: p. 1-9.
- [19] Rezaeiha, A., I. Kalkman, and B. Blocken, *Effect of pitch angle on power performance and aerodynamics of a vertical axis wind turbine*. *Applied Energy*, 2017. **197**: p. 132-150.
- [20] Rezaeiha, A., I. Kalkman, H. Montazeri, and B. Blocken, *Effect of the shaft on the aerodynamic performance of urban vertical axis wind turbines*. *Energy Conversion and Management*, 2017. **149**: p. 616-630.
- [21] Alaimo, A., A. Esposito, A. Messineo, C. Orlando, and D. Tumino, *3D CFD Analysis of a Vertical Axis Wind Turbine*. *Energies*, 2015. **8**(4): p. 3013-3033.
- [22] Araya, D.B. and J.O. Dabiri, *A comparison of wake measurements in motor-driven and flow-driven turbine experiments*. *Experiments in Fluids*, 2015. **56**(7).
- [23] Armstrong, S., A. Fiedler, and S. Tullis, *Flow separation on a high Reynolds number, high solidity vertical axis wind turbine with straight and canted blades and canted blades with fences*. *Renewable energy*, 2012. **41**: p. 13-22.
- [24] Möllerström, E., S. Eriksson, A. Goude, F. Ottermo, and J. Hylander, *Turbulence influence on optimum tip speed ratio for a 200 kW vertical axis wind turbine*. *Journal of Physics: Conference Series*, 2016. **753**: p. 032048.
- [25] Paraschivoiu, I. and P. Desy, *Aerodynamics of small-scale vertical-axis wind turbines*. *Journal of Propulsion and Power*, 1986. **2**(3): p. 282-288.
- [26] Parker, C.M. and M.C. Leftwich, *The effect of tip speed ratio on a vertical axis wind turbine at high Reynolds numbers*. *Experiments in Fluids*, 2016. **57**(5).
- [27] Ahmadi-Baloutaki, M., D.S.K. Ting, and R. Carriveau, *The Role of Free-Stream Turbulence on Flow Evolution in the Wake of a VAWT Blade*. *Wind Engineering*, 2013. **37**(4): p. 401-420.
- [28] Möllerström, E., F. Ottermo, A. Goude, S. Eriksson, J. Hylander, and H. Bernhoff, *Turbulence influence on wind energy extraction for a medium size vertical axis wind turbine*. *Wind Energy*, 2016. **19**(11): p. 1963-1973.
- [29] Siddiqui, M.S., A. Rasheed, T. Kvamsdal, and M. Tabib, *Effect of Turbulence Intensity on the Performance of an Offshore Vertical Axis Wind Turbine*. *Energy Procedia*, 2015. **80**: p. 312-320.
- [30] Bachant, P. and M. Wosnik, *Effects of Reynolds Number on the Energy Conversion and Near-Wake Dynamics of a High Solidity Vertical-Axis Cross-Flow Turbine*. *Energies*, 2016. **9**(2): p. 73.
- [31] Blackwell, B.F., R.E. Sheldahl, and L.V. Feltz, *Wind tunnel performance data for the Darrieus wind turbine with NACA 0012 blades*. 1976, Office of Scientific and Technical Information (OSTI).
- [32] McLaren, K., S. Tullis, and S. Ziada, *Measurement of high solidity vertical axis wind turbine aerodynamic loads under high vibration response conditions*. *Journal of Fluids and Structures*, 2012. **32**: p. 12-26.
- [33] Polagye, B.L., R.J. Cavagnaro, and A.L. Niblick, *Micropower From Tidal Turbines*, in *Volume 1B, Symposia: Fluid Machinery; Fluid Power; Fluid-Structure Interaction and Flow-Induced Noise in Industrial Applications; Flow Applications in Aerospace; Flow Manipulation and Active Control: Theory, Experiments and Implementation; Fundamental Issues and Perspectives in Fluid Mechanics*. 2013, ASME.
- [34] McLaren, K.W., *A numerical and experimental study of unsteady loading of high solidity vertical axis wind turbines*. 2011.
- [35] Elkhoury, M., T. Kiwata, and E. Aoun, *Experimental and numerical investigation of a three-dimensional vertical-axis wind turbine with variable-pitch*. *Journal of Wind Engineering and Industrial Aerodynamics*, 2015. **139**: p. 111-123.
- [36] Li, Q.a., T. Maeda, Y. Kamada, J. Murata, M. Yamamoto, T. Ogasawara, K. Shimizu, and T. Kogaki, *Study on power performance for straight-bladed vertical axis wind turbine by field and wind tunnel test*. *Renewable Energy*, 2016. **90**: p. 291-300.

- [37] Rezaeiha, A., H. Montazeri, and B. Blocken, *Towards optimal aerodynamic design of vertical axis wind turbines: Impact of solidity and number of blades*. Energy, 2018. **165**: p. 1129-1148.
- [38] Lohry, M.W. and L. Martinelli, *Unsteady Reynolds-Averaged Navier–Stokes Simulation of Crossflow Rotors, Scaling, and Blockage Effects*. AIAA Journal, 2016. **54**(12): p. 3828-3839.
- [39] Bhargav, M., V.R. Kishore, and V. Laxman, *Influence of fluctuating wind conditions on vertical axis wind turbine using a three dimensional CFD model*. Journal of Wind Engineering and Industrial Aerodynamics, 2016. **158**: p. 98-108.
- [40] Chandramouli, S., T.P. Premsai, P. Prithviraj, V. Mugundhan, and R.K. Velamati, *Numerical analysis of effect of pitch angle on a small scale vertical axis wind turbine*. International Journal of Renewable Energy Research (IJRER), 2014. **4**(4): p. 929-935.
- [41] Bedon, G., M.R. Castelli, and E. Benini, *Optimal spanwise chord and thickness distribution for a Troposkien Darrieus wind turbine*. Journal of Wind Engineering and Industrial Aerodynamics, 2014. **125**: p. 13-21.
- [42] Bedon, G., M.R. Castelli, and E. Benini, *Proposal for an innovative chord distribution in the Troposkien vertical axis wind turbine concept*. Energy, 2014. **66**: p. 689-698.
- [43] Delafin, P.L., T. Nishino, A. Kolios, and L. Wang, *Comparison of low-order aerodynamic models and RANS CFD for full scale 3D vertical axis wind turbines*. Renewable Energy, 2017. **109**: p. 564-575.
- [44] Qamar, S.B. and I. Janajreh, *Investigation of effect of cambered blades on Darrieus VAWTs*. Energy Procedia, 2017. **105**: p. 537-543.
- [45] Meana-Fernández, A., I. Solís-Gallego, J.M.F. Oro, K.M.A. Díaz, and S. Velarde-Suárez, *Parametrical evaluation of the aerodynamic performance of vertical axis wind turbines for the proposal of optimized designs*. Energy, 2018. **147**: p. 504-517.
- [46] Rezaeiha, A., H. Montazeri, and B. Blocken, *On the accuracy of turbulence models for CFD simulations of vertical axis wind turbines*. Energy, 2019. **180**: p. 838-857.
- [47] Benzerdjeb, A., M.K. Hamidou, B. Abed, M. Bordjane, H. Achache, and A.M. Gorlov. *Numerical study on the performance of darrieus turbine by K-ε standard and K-ε EARSM turbulence models*. in 2017 IEEE 6th International Conference on Renewable Energy Research and Applications (ICRERA). 2017.
- [48] Goodfield, D., S.P. Evans, A. Kc, D.R. Bradney, T.P. Urmee, J. Whale, and P.D. Clausen, *The suitability of the IEC 61400-2 wind model for small wind turbines operating in the built environment*. Renewable Energy and Environmental Sustainability, 2017. **2**: p. 31.
- [49] Tummala, A., R.K. Velamati, D.K. Sinha, V. Indrāja, and V.H. Krishna, *A review on small scale wind turbines*. Renewable and Sustainable Energy Reviews, 2016. **56**: p. 1351-1371.
- [50] Kaadan, A.T., M. Endo, M. Uruta, and T. Yasuda. *Implementation of VAWT in Energy Generation Decentralization in Developing Countries Social, Engineering & Open Data case study in South-East Asia*. in 2018 7th International Conference on Renewable Energy Research and Applications (ICRERA). 2018.